Hybrid Hydrogel-Magnet Actuated Capsule for Automatic Gut Microbiome Sampling

Yung P. Lai, Taeyoung Lee, Daniel Sieben, Lyle Gauthier, Jaekwang Nam, and Eric Diller, *Senior Member, IEEE*

***Abstract*— Objective: Non-invasive, pill-sized capsules can provide intestinal fluid sampling to easily retrieve site-specific gut microbiome samples for studies in nutrition and chronic diseases. However, capsules with both automatic sampling and active locomotion are uncommon due to limited onboard space. This paper presents a novel hybrid hydrogel-magnet actuated capsule featuring: i) pH-responsive hydrogels that will automatically trigger fluid sampling at an environmental pH of $>$ 6 and ii) active locomotion by an external rotating magnetic field. Method: Two capsule designs were fabricated (Design A: 31 μL sampling volume with dimensions 8 mm $\times$ 19 mm, Design B: 41 μL sampling volume with dimensions 8 mm $\times$ 21 mm). They were immersed in simulated gastric (pH = 1.2) and simulated intestinal fluid (pH = 6.8) to test for automatic intestinal fluid sampling. An external rotating magnetic field was applied to test for active locomotion. Finally, seal tests were performed to demonstrate sample contamination mitigation. Results: Preliminary experiments showed that sampling occurred quickly and automatically in simulated intestinal fluid at 6 - 15 hours, active locomotion via rotation, rolling, and tumbling were possible at magnetic field magnitudes $<$ 10 mT, oil piston seals were better at mitigating sample contamination than water piston seals, and minimum o-ring seal pressures limits of 1.95 and 1.69 kPa for Design A and B respectively were sufficient against intra-abdominal pressures. Significance: This work presents the ability to impart capsule multi-functionality in a compact manner without onboard electronics or external triggering for sampling.**

***Index Terms*— wireless capsule, hydrogel actuators, magnetic mechanism, medical robotics**

I. Introduction

THE human gut microbiome is composed of a vast and diverse microbial population that live in symbiosis [1]. Its composition and metabolic pathways have been shown to be important markers of disease (e.g., cancer, diabetes, and inflammatory bowel disease (IBD)) [1, 2]. To study the gut microbiome, methods such as stool sampling, ileostomy, or colonoscopy are currently used. In stool sampling, stools are analyzed for their genetic content via 16S ribosomal RNA or DNA techniques and other metagenomic methods. However, stools provide inadequate information on site-specific microbiome populations in the intestines. Alternatively, ileostomies and colonoscopies provide site-specific sampling, but are highly invasive. Thus a non-invasive sampling tool which can perform targeted sampling within the small intestine is needed.

Ingestible capsules provide a solution for site-specific minimally invasive microbiome sampling. The ingestible size of the capsules enables access to remote and tortuous regions which are often difficult to reach with tethered alternatives [3]. Existing ingestible capsules can capture images [4], conduct tissue biopsies [5–8], perform drug delivery [9–11], and perform active locomotion [12, 13]. Existing fluid sampling capsules come with limitations depending on the approach. Two major approaches have been attempted for fluid sampling in the capsule.

In the active fluid sampling approach, onboard batteries have been used to drive piston pumps [9, 14] or opening of a hinged door actuated by a shape memory alloy spring [15]. However, due to the presence of onboard batteries and electronics, the capsule sizes were large (Table I). Capsules with active sampling and without onboard power have been designed using magnetic actuation to activate a hinge door, piston pump, or rotating trapdoor via an external magnetic field [16–20]. However, knowledge of the capsule location is generally required for magnetic actuation. Moreover, knowing when to activate sampling is challenging with a large chance of triggering sampling erroneously within the stomach due to uncertain gastric transit times. Novel actuators which can automatically actuate themselves for passive sampling once the capsule has reached the small intestine should be considered to avoid the need for complex external guidance, control and actuation.

In the passive approach, temperature-responsive materials have been used to trigger mechanisms, but endoscopically delivered water with a temperature of 55°C was required [24]. Otherwise, biocompatible, pH-responsive hydrogels or enteric coatings can be used to trigger mechanisms at the desired sampling region by leveraging the large pH change between the stomach and small intestine. Hydrogels can also provide

Manuscript received 25 May 2023; revised 13 January 2024; accepted 7 May 2024. This work was supported in part by the Natural Sciences and Engineering Research Council of Canada [RGPIN-2020-04551]. (Corresponding author: Eric Diller.)

Y.P. Lai, T. Lee, D. Sieben, and L. Gauthier are with the Department of Mechanical and Industrial Engineering, University of Toronto, Toronto, Canada (e-mail: yp.lai@mail.utoronto.ca, taeyoungty.lee@mail.utoronto.ca, daniel.sieben@mail.utoronto.ca, gauthier@mie.utoronto.ca).

E. Diller is with the Robotics Institute, the Institute for Biomedical Engineering, and the Department of Mechanical and Industrial Engineering, University of Toronto, Canada (email: eric.diller@utoronto.ca).

J. Nam is with the School of Robotics, Kwangwoon University, Seoul, South Korea (e-mail: jk2020@kw.ac.kr).

TABLE I
COMPARISON OF ACTIVE AND PASSIVE FLUID SAMPLING CAPSULES

	Sampling Mechanism	Actuation Method	Diameter × Length (mm × mm)	Sampling Time	Active Locomotion Reported	Ref.
Active	Pump	Motorized pump	10.2 × 30	On-demand	x	[9]
	Hinge door	SMA spring	12 × 45	On-demand	x	[15]
	Hinge door	Magnetic	8 × 11	On-demand	✓	[16]
	Hinge door	Magnetic	12.4 × 26	On-demand	x	[17]
	Micropump	Magnetic	11 × 26	On-demand	✓	[18]
	Brushes	Magnetic	11.5 × 30	On-demand	x	[20]
	Absorption with rayon	Heat/magnetic	11 × 26	Not reported	✓	[19]
Passive	Foam swelling	Foam	9 × 26	3 - 4 min	x	[21]
	Hydrogel swelling	Hydrogel	9× 15 and 7×11	6 hr	x	[22, 23]
	Sliding micropiston	pH-responsive hydrogel/magnetic	8 × 19 and 8 × 21	< 5 s	✓	This work

SMA = Shape memory alloy

large displacements as actuators [22, 25–28] and can be easily miniaturized to small size scales [25].

Previous works have used hydrogels or foams to actuate mechanisms in capsules in the small intestine [21–23, 28, 29]. In one study, the pH-responsive hydrogel triggered an electric switch, but the embedded electronics made the capsule bulky (9 mm × 22 mm) [28]. For fluid sampling capsules using non-pH-responsive hydrogels or foams, enteric coatings were required as an initial seal to prevent premature sampling in the stomach [21–23, 29]. Furthermore, these capsules' sampling and closing mechanisms were highly dependent on the hydrogel swelling rate. The sampling compartment was also exposed to environmental fluid for 3 - 4 minutes to an hour while the capsule would passively move along the small intestine depending on the capsule design. Moreover, by relying on the hydrogel itself to store the sample, a sample extraction step from the hydrogel will need to be performed prior to microbiome analysis as seen in [23]. The added extraction procedure adds an extra step in the capsule workflow and another set of protocol will be required to ensure high sample extraction. No hydrogel actuated fluid sampling capsules have a separate sampling compartment from the hydrogel to trigger sampling and closing mechanisms. Furthermore, no active or passive fluid sampling capsules have features to avoid sampling in the undesired gastric region without using enteric coating and also demonstrate active locomotion (Table I).

This paper presents a capsule that separates the sampling compartment from the hydrogel. In doing so, the sampling and closing rate of the capsule is no longer dependent on the hydrogel swelling rate. Moreover, an independent sampling compartment from the hydrogel will allow for easy sample retrieval prior to microbiome analysis. The pH-responsive hydrogel will automatically sense and trigger the capsule mechanism in the small intestine, thus avoiding sampling in the undesired gastric region. The magnets within the capsule drive the sampling and closing mechanism and can also be used for capsule locomotion under an external rotating magnetic field. Finally, the capsule also fulfills three major design requirements for human gut microbiome retrieval. First, the capsule size should be within 11 mm × 26 mm, the FDA approved size for ingestible capsule endoscopes for adults and children 10 years and older [30]. Second, fluid sampling should occur without external activation. Lastly, the capsule should be sealed after collection to prevent contamination/leakage. The following sections introduce the capsule concept, identifies design parameters for high-performance capsule designs within size limits, demonstrate automatic simulated intestinal fluid (SIF) sampling at a pH of 6.8, explore different active locomotion modes, and investigate seal performance to show the capsule's ability to resist leakage and contamination from the surrounding fluid.

II. CAPSULE CONCEPT

The capsule goes through a series of states (closed-open-sampling-closed). Sampling occurs when the capsule opens and an activated piston creates a suction force for sample collection at an environmental pH > 6. To enable this behavior, the capsule body is composed of independent upper and lower halves, as seen in Fig. 1a and Fig. 1b. The upper half is comprised of the end cap, latch magnet, pH-responsive hydrogel, hydrogel compartment, sliding component, and two small cubic spring magnets. The lower half is comprised of the Mold Star 30 o-ring seal, the piston magnet, the sampling compartment lid, the sampling compartment, the activating magnet, and the activating magnet fixture. The two halves can slide past another to open and close the capsule. To ensure the capsule can close after it opens, the two halves are connected by a string tied onto the piston magnet and glued to the top of the sliding component.

The assembled capsule houses a total of five magnets, which act as latches and springs to allow the components to snap between open/closed states. The major magnetic component in the capsule is three diametrically magnetized magnets that are aligned along the vertical axis of the capsule (Fig. 1c). The first magnet acts as a latch, while the second magnet acts as a piston and is connected to the upper half of the capsule body with a string. The third magnet serves two functions, primarily as an activating magnet and as a spring magnet. Two smaller diametrically magnetized spring magnets are located near the base of the capsule and are placed on opposite sides of the capsule body (Fig. 1b). Intestinal fluid can travel into the hydrogel compartment through the end cap and the rectangular channel at the bottom of the hydrogel compartment. The hydrogel is placed in the middle of the rectangular channel where it can swell (Fig. 1c). The hydrogel is an agar and

This article has been accepted for publication in IEEE Transactions on Biomedical Engineering. This is the author's version which has not been fully edited and content may change prior to final publication. Citation information: DOI 10.1109/TBME.2024.3401681

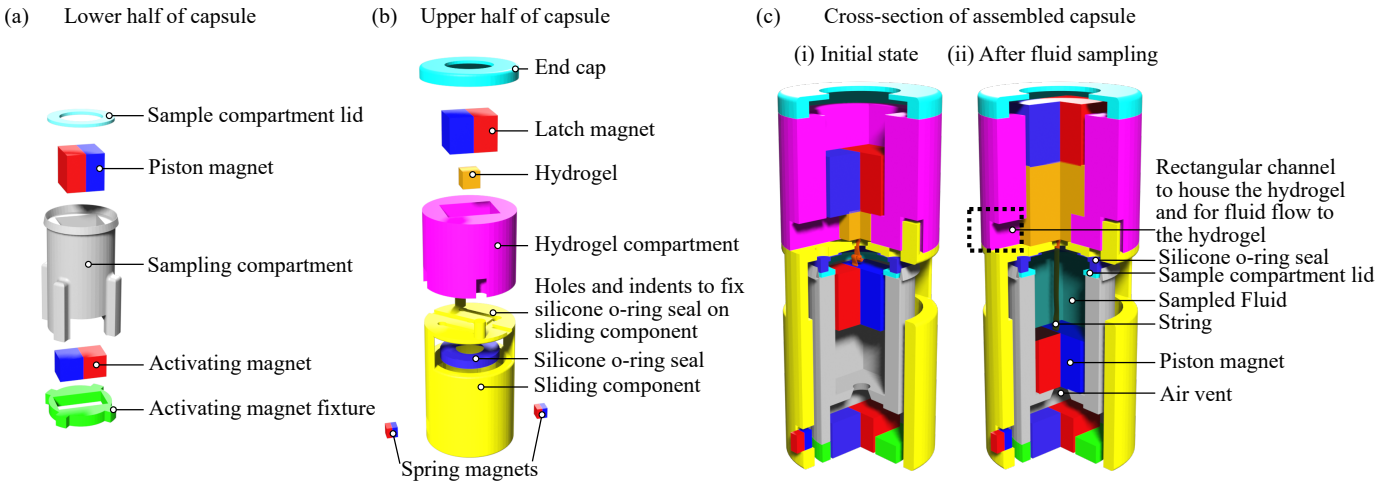

Fig. 1. Exploded view of the (a) lower half of the capsule, (b) upper half of the capsule, and (c) cross-section of the assembled capsule in its initial state and closed state after fluid sampling where the air vent and string connecting the piston magnet to the sliding component are shown. The capsule mechanism is shown in detail in Fig. 2, and component motions are visualized in the Supplementary Video 1.

poly(acrylic acid) interpenetrating network hydrogel and UV cured into a 1.5 mm cube as described in [31].

When the capsule is fully assembled, there are only three major moving parts (refer to Supplementary Video 1): (i) the latch magnet can slide when the hydrogel starts to swell, (ii) the piston magnet can slide in the sampling compartment for sampling, and (iii) the entire upper half of the capsule can slide past the entire lower half of the capsule when the capsule opens for sampling. All other fixed parts were glued together with cyanoacrylate glue except for the silicone o-ring. The o-ring was cured in place on the sliding component by applying a thin layer of silicone rubber in the hole and indents on the other side of the sliding component as seen in Fig. 1b. All other structural components were printed with Clear V4 resin with the Form3 3D printer (FormLabs Inc.).

III. Capsule Mechanism Design

The capsule travels through 3 different environments (initial, stomach, and small intestine), where the state is either closed, open, or sampling as illustrated in Fig. 2a and 2d. The latch magnet initially engages the piston magnet through an attractive magnetic force which holds the piston magnet in place and prevents it from sliding down the sampling compartment keeping the capsule closed (Fig. 2d, step 1).

In the stomach's acidic environment, the hydrogel will swell slightly, but the hydrogel displacement is small and does not trigger the magnetic mechanism (Fig. 2d, step 2). Thus, the capsule remains closed in the stomach. Through the natural peristaltic contractions of the gut, the capsules will move into the small intestine (Fig. 2d, step 3). The hydrogel will undergo large volume transition in the intestinal pH of approximately 6.8, which will displace the latch magnet away from the piston magnet.

At the critical hydrogel height (h_{crit}), the latch magnet eventually disengages from the piston magnet due to decreasing magnetic interaction force at the further distance. Consequently, the spring force from the spring magnets can overcome the latching force and slide the capsule open (Fig. 2d, step 4 and 5). At the same time, the latching force becomes negligible and the activating magnet's attractive force will be able to pull the piston magnet down the sampling compartment (Fig. 2d, step 6). As the piston magnet slides down, fluid is sampled from the opening in the middle of the capsule. Any trapped air bubbles in the sampling compartment are expelled from the air vent at the bottom. Once the piston magnet slides to the end of the sampling compartment, the string will pull the upper half of the capsule towards the lower half and close the capsule (Fig. 2d, step 7). Thus, fast sampling and closing with pH-responsive hydrogel can be achieved with no external activation and the capsule exits the body by excretion. A timeline of the expected transit time in the stomach and small intestine and the expected duration of capsule opening, sampling, and closing is shown in Fig. 2d.

A. Magnetic Modeling

To design the capsule with the desired closed-open-sampling-closed mechanism, magnetic force analysis was conducted on each magnet. Magnetic forces were calculated using the dipole model shown in (1).

$$\mathbf{F_{ab}} = \frac{3\mu_0}{4\pi r^5}\left[(\mathbf{m_a}\cdot\mathbf{r})\mathbf{m_a} + (\mathbf{m_b}\cdot\mathbf{r})\mathbf{m_a} + (\mathbf{m_a}\cdot\mathbf{m_b})\mathbf{r} - \frac{5(\mathbf{m_a}\cdot\mathbf{r})(\mathbf{m_b}\cdot\mathbf{r})}{r^2}\mathbf{r}\right], \quad (1)$$

where $\mathbf{m_a}$ and $\mathbf{m_b}$ are the magnetic moment of the permanent magnet dipoles, $\mathbf{r}$ is the vector between the two magnetic dipoles, and μ_0 is the vacuum permeability. The dipole model has been shown to provide a good magnetic force approximation for cube magnets [32] and the magnets' geometries in this work were either cubes or rectangular prisms. All magnet volumes were also evenly divided into at least 100 dipoles along its height and width to obtain a more accurate representation of the magnetic force at small distances between the magnets. The sum of all the forces among the dipoles was

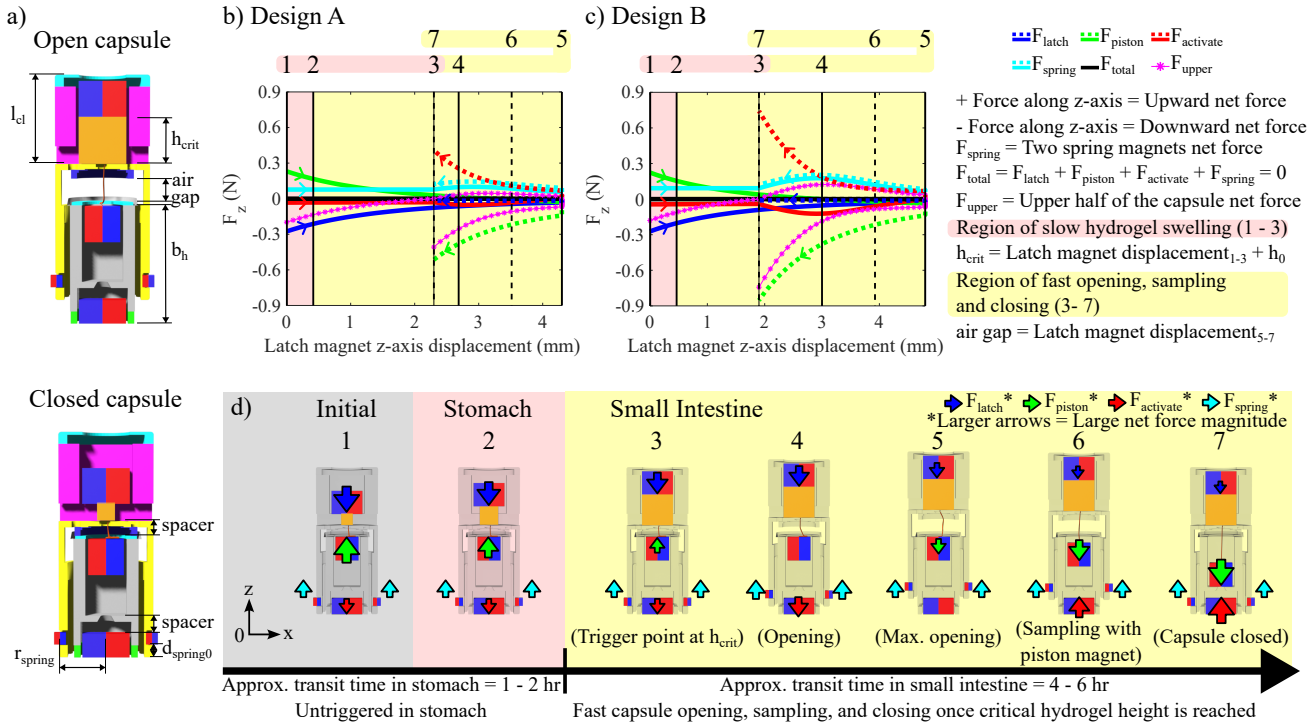

Fig. 2. (a) Open capsule at maximum opening height and closed capsule with important capsule parameters labelled and described in Table II. (b) Predicted net force along the z-axis vs. latch magnet displacement curves for the latch, piston, activating, spring magnets, and upper half of the capsule for Design A. (c) Predicted net force along the z-axis vs. latch magnet displacement curves for the latch, piston, activating, spring magnets, and upper half of the capsule for Design B. (d) The corresponding capsule configurations in the stomach and small intestine are shown along with the proposed capsule timeline in the stomach and in the small intestine.

TABLE II
CAPSULE PARAMETERS FOR DESIGN A AND DESIGN B

Capsule parameters	Design A	Design B
Total capsule length (mm)	19	21
Activating magnet dimensions (mm)	2 ×4 × 2	3 ×4 × 3
b_h (mm)	10	12
$d_{spring0}$ (mm)	1.2	1.6
Piston magnet dimensions	3 mm cube	
Spring magnet dimensions	1 mm cube	
Latch magnet dimensions (mm)	3 ×4 × 3	
r_{spring} (mm)	3.9	
Capsule OD (mm)	8	
l_{cl} (mm)	7.5	
spacer (mm)	1.5	
h_0 (mm)	1.5	

Note: Remanence (B_r) = 1.44 T for all N50 magnets (SuperMagnetMan Inc.). All magnet dimensions are length × width × height unless otherwise specified. b_h - base height, $d_{spring0}$ - initial spring magnet z position, r_{spring} - distance from the center of the activating magnet to the center of the spring magnet, OD - outer diameter, l_{cl} - hydrogel compartment and lid height, h_0 - initial hydrogel height.

TABLE III
LIST OF CONSTRAINTS TO ENSURE THE MECHANISM FUNCTIONS AS INTENDED

Step in Fig. 2d	Constraints
1. Initial	$F_{activate} \leq$ -30 mN
1. Initial	$F_{spring} \geq$ 30 mN
1. Initial	$F_{piston} \geq$ 30 mN
2. Stomach	$\lambda_{crit} \geq 1.74$
3. Critical hydrogel height	$F_{piston} > 0$ mN
3 - 5. Opening	air gap ≥ 0 mm
4. Opening	$F_{max\ spring} \geq$ 50 mN
5. Max. opening	$F_{piston} < 0$ mN
5 - 7. Sampling and closing	$F_{activate} \geq 0$ mN for all activating magnet positions between 5 - 7

λ_{crit} - ratio of the critical hydrogel height (h_{crit}) to the initial dry hydrogel height (h_0).

the magnetic force between two magnets. The net magnetic forces of each magnet in the capsule were calculated by summing all magnetic forces ($\mathbf{F_{ab}}$) acting on each magnet.

The critical hydrogel height (h_{crit}) and air gap are dependent on the magnetic forces within the capsule. h_{crit} is the hydrogel height right before the capsule starts to open (i.e., h_0 + latch magnet displacement between step 1 to step 3, Fig. 2b and Fig. 2c). The air gap is estimated to be the latch magnet displacement from step 5 to step 7, (Fig. 2b and Fig. 2c) assuming hydrogel height remains relatively constant between steps 3 - 7.

B. Grid Search of the Design Space

Two capsule designs were fabricated in this paper to demonstrate the capsule's capabilities. Design A and B were based on solutions from a grid search of the capsule design space. The parameters of the grid search were latch and activating magnet dimensions, initial spring magnet height from the base of the capsule ($d_{spring0}$), and base height of the capsule (b_h, Fig. 2a). The constants in the design were the piston magnet dimensions, spring magnet dimensions, distance from the center of the activating magnet to the center of the spring magnet (r_{spring}), capsule outer diameter, hydrogel compartment and lid height (l_{cl}), spacer, initial dry hydrogel height (h_0),

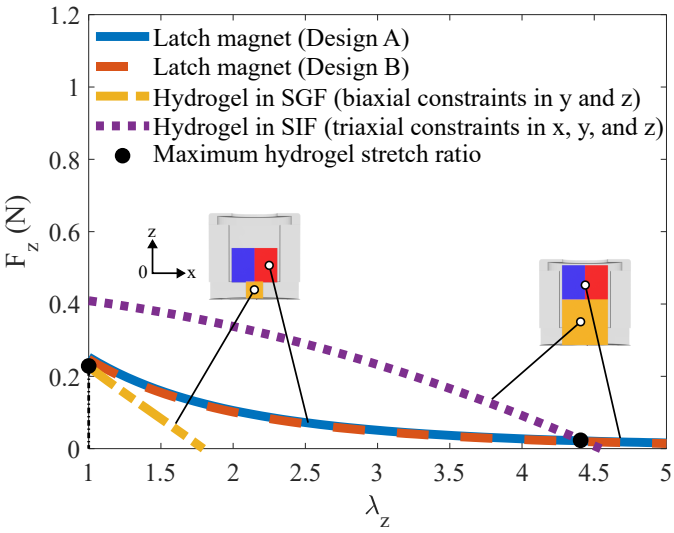

Fig. 3. Comparison of predicted net latch magnet forces (3 × 4 × 3 mm cube N50 magnet) of Design A and B with predicted hydrogel forces at equilibrium in SGF and SIF (1.5 mm cube hydrogel) vs. hydrogel stretch ratio in the z-direction (i.e., ratio of hydrogel height at equilibrium to initial dry hydrogel height). The hydrogels undergo biaxial wall constraints in SGF (w_y = 1) and triaxial wall constraints in SIF (w_x = 4.5/1.5 w_y =3.5/1.5) due to the hydrogel compartment structure. The maximum λ_z in SGF and SIF is when F_z is zero. The maximum blocking force of the hydrogel is when λ_z = 1.

magnet magnetization directions, and remanence (B_r) (Table II). Magnetic force displacement curves for each parameter combination were calculated (e.g. Fig. 2b and Fig. 2c). The forces from the curves had to satisfy a set of magnetic force constraints to ensure a functional capsule was obtained (Table III). The result of the grid search was a list of parameter combinations that resulted in a functional closed-open-sampling-closed mechanism. Design A had the smallest base height from the exploratory grid search of the design space. Design B had the largest predicted magnetic spring force in the design space. The capsule design parameters and dimensions for both designs are listed in Table II.

C. Hydrogel Modeling

The magnetic force modeling in the previous section was used to determine combination of design parameters that would result in a functional mechanism. The hydrogel modeling in this section would help determine if there is sufficient hydrogel force to push apart the latch and piston magnet and to determine whether the mechanism would be triggered in intestinal fluid. The agar-poly(acrylic acid) hydrogel undergoes an abrupt change in volume at pH $>$ 6 as studied in [31]. The maximum hydrogel swelling in simulated gastric and simulated intestinal fluid (SGF and SIF respectively) at equilibrium can be estimated by a free energy function [31]. When the hydrogel is constrained by walls, its vertical swelling will be larger than when it is unconstrained which also needs to be accounted for. Based on the geometry of the hydrogel compartment, the hydrogel undergoes biaxial wall constraints in SGF (y and z directions, Fig. 3). The other lateral direction (x-direction), acts as an unconstrained direction because there is a rectangular channel for fluid flow that allows the hydrogel to swell through (Fig. 1c) and hydrogel swelling in SGF is small. In SIF, the hydrogel will undergo large volume transition and will eventually undergo triaxial wall constraints because of hydrogel compartment's rectangular cross-section geometry (Fig. 3). The wall constraints for the hydrogel in the x and y direction are given as a ratio of the hydrogel compartment length over initial hydrogel height of, w_x = 4.5/1.5 and w_y = 3.5/1.5). More information of these wall constraint values in the calculation of the predicted hydrogel force at equilibrium can be found in [31].

In SGF, both the net latch magnet forces in Design A and B are greater than the maximum hydrogel forces in SGF for an initially 1.5 mm cube hydrogel (Fig. 3). Therefore, in SGF, the hydrogel would not have sufficient blocking force to push on the latch magnet for both designs. The estimated hydrogel stretch ratio (λ_z) would be 1, i.e., hydrogel height would not change in SGF. Thus, sampling does not occur in SGF. In SIF, the net latch magnet forces were less than the hydrogel forces until a maximum hydrogel stretch ratio of around 4.4 (Fig. 3). Therefore, the estimated maximum hydrogel stretch ratio in SIF at equilibrium was around 4.4 for both Design A and B. From these stretch ratios, the maximum hydrogel height in SGF and SIF given an h_0 of 1.5 mm would be 1.5 mm and 6.6 mm respectively.

To ensure the mechanism always triggers in the small intestine with a pH of 6.8, h_{crit} should be between the estimated maximum hydrogel height in SGF and SIF. From magnetic force calculations, h_{crit} can be tuned by adjusting the magnet position and dimensions in the capsules. From Fig. 2b and Fig. 2c, the h_{crit} of Design A and B were 3.8 and 3.4 mm respectively. These values are between the calculated maximum hydrogel height in SGF and SIF. Therefore, the mechanism will only trigger in intestinal fluid.

IV. Experiments

A. Verification of Magnetic Modeling

A fixture was fabricated to confirm that the dipole magnetic model was accurate when predicting h_{crit}. The jig was designed such that there was minimal friction on the piston and activating magnet component as it slid past the spring magnets and only simulates the magnets' positions relative to each other in the capsule. The two 1 mm spring cube magnets were placed at the north and south poles of the activating magnet at approximately 3.9 mm from the activating magnet's center of the mass (COM) shown in Fig. 4a.

The distance between the piston and activating magnet was arbitrarily fixed to a base height of 16 mm. Initially, the piston magnet was held in place magnetically by the latch magnet and separated by a 0.5 mm spacer. The latch magnet was then slowly moved away from the piston magnet. When the piston magnet disengaged from the latch magnet, the distance between the base of the latch magnet to the top of the spacer was measured using a caliper. The measured distance was the critical hydrogel height that triggered the opening mechanism.

The results demonstrated that the experimental h_{crit} was comparable to the h_{crit} calculated by the magnetic dipole model especially at larger initial spring magnet distances since the

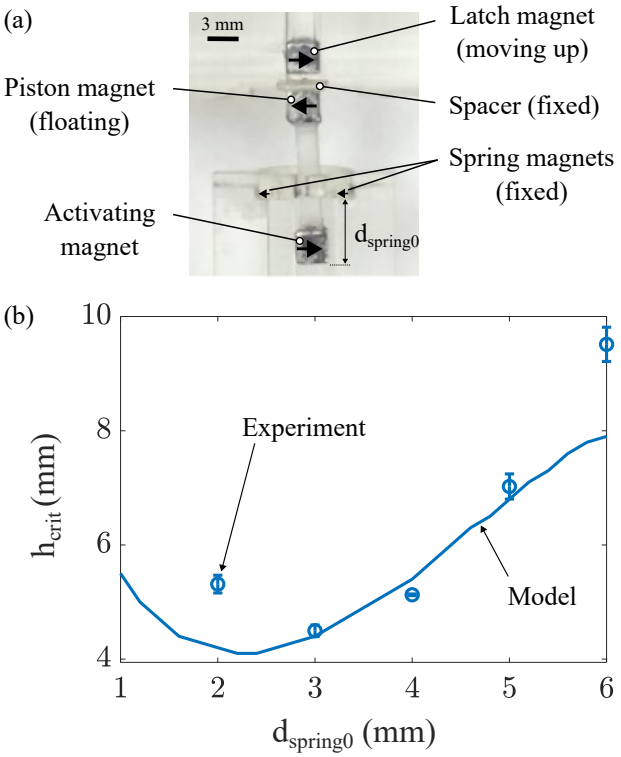

Fig. 4. (a) Experimental setup of the jig to estimate the critical hydrogel height of the capsule design. The black arrows represent the magnets' magnetization directions. The jig simulates the latch, piston, spring, and activating magnet positions relative to each other in the capsule so no other actual capsule components are included. The $d_{spring0}$ is fixed and the latch magnet is slowly translated vertically to determine the critical hydrogel height at which the piston magnet disengages from the latch magnet. (b) Critical hydrogel height (h_{crit}) vs. initial spring magnet position ($d_{spring0}$) (n = 3 for all data points, error bars are standard deviation). Spring magnets are 1 mm cube magnets.

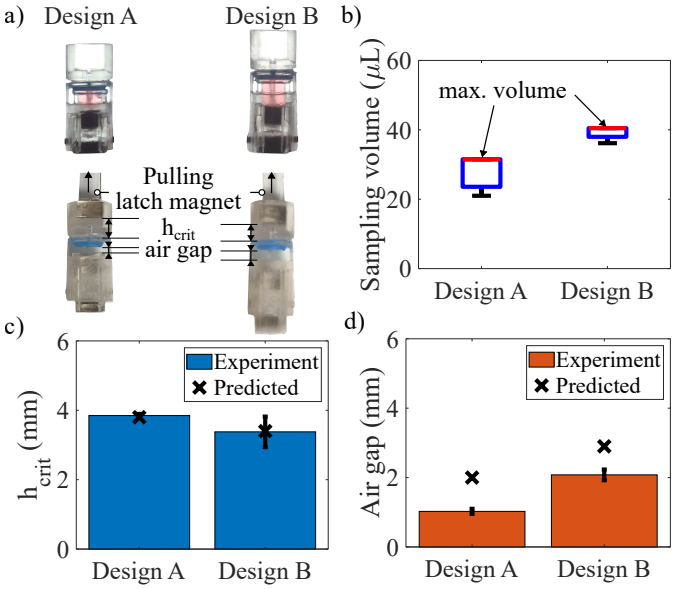

Fig. 5. (a) Design A and B with sampled red-dyed water to determine sampling volumes and manually triggered Design A and B to determine critical hydrogel height (h_{crit}) and the air gap. (b) Sampling volume of manually triggered Design A and B (n = 5, error bars are standard deviation). (c) Manually triggered Design A and B and the predicted and measured critical hydrogel height (h_{crit}, n = 3, error bars are standard deviation) and (d) the predicted and measured air gap (n = 3, error bars are standard deviation).

dipole model is most accurate at larger distances between magnetic dipoles (Fig. 4b). The jig was designed to minimize frictional forces, but it may still be present. The friction and measurement error may explain some of the discrepancy between experimental data and dipole model.

B. Manually Actuated Capsule: Sampling Volume, h_{crit}, and Air Gap

To demonstrate the repeatability of the sampling volume, the sampling mechanism, and the real-time speed of the sampling and closing mechanism, Design A and B were manually triggered by attaching the latch magnet to a rod. The rod was slowly pulled away from the piston magnet to simulate latch magnet displacement when the hydrogel swells. The capsules were immersed in red-dyed water for manually triggered fluid sampling and recorded on camera (Supplementary Video 2). Any trapped air bubbles in the sampling compartment appeared to take a semi-ellipsoid shape after sampling was completed. The ellipsoid was assumed to have a circular base. The diameter and height of the bubble in the image was measured and subtracted from the known maximum volume of the fluid sampling compartment to estimate the total sampling volume of the capsule. Since Design A had a smaller capsule height, its sampling volume ranged from 21 - 31 µL (n = 5) while Design B had a slightly larger sampling volume ranging from 36 - 41 µL (n = 5) (Fig. 5b). Air bubbles can become trapped in the compartment after sampling because of the unevenly distributed oil seal applied around the piston magnet, resulting in lower piston suction performance. The sampling volumes for the current capsule design should be sufficient for genetic analysis of microbiome populations as the BCMAC in [16] was able to extract DNA from 18 to 61 mg of sample. Moreover, previous literature shows DNA extraction is dependent on the efficiency of the DNA extraction kits [33]. DNA extraction was possible from 10 - 50 mg of fecal sample [33]. Assuming the sampled fluid has the density of water (1 $g{\cdot}mL^{-1}$) and that the capsule is fully filled, the current sampling volume of 21 - 41 µL will sample 21 and 41 mg respectively. Accordingly, the sampling volume would be sufficient.

Design A and B were then taped onto a surface and manually triggered to determine h_{crit} and the air gap at capsule activation. Design A and B had a predicted h_{crit} of 3.8 and 3.4 mm respectively and a predicted air gap of 2 and 2.9 mm respectively (values from Fig. 2b and Fig. 2c). Measured h_{crit} in Fig. 5c were close to predicted h_{crit} values (3.85 $\pm$ 0.05 mm vs. 3.38 $\pm$ 0.45 mm, n = 3, mean $\pm$ standard deviation for Design A and B respectively). However, measured air gap values in Fig. 5d were not similar to predicted values (1.03 $\pm$ 0.07 mm vs. 2.08 $\pm$ 0.15 mm, n = 3, mean $\pm$ standard deviation for Design A and B respectively). Deviations between air gap predictions with experimental data in Fig. 5d were likely due to unaccounted friction in the sliding mechanism and imperfections in fabrication. However, Design B consistently had larger predicted and measured air gaps than Design A due

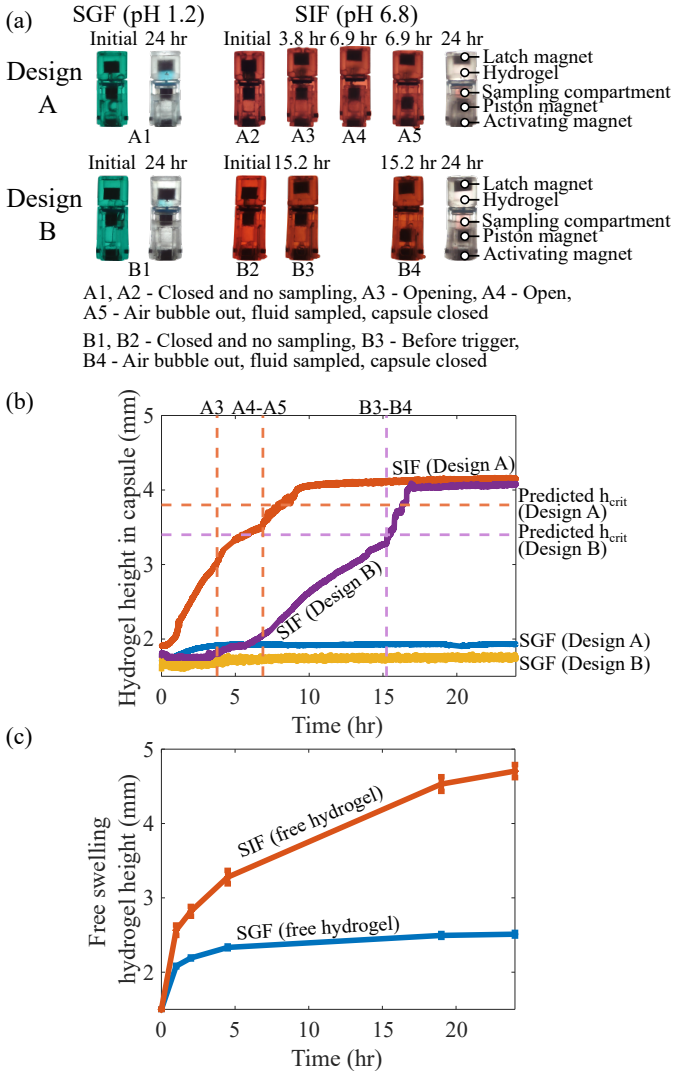

Fig. 6. (a) Hydrogel actuated Design A and Design B immersed in SGF and SIF and their respective capsule states. (b) Hydrogel height vs. time in SGF and SIF for Design A and B and their respective trigger times and predicted critical hydrogel height at the trigger time. (c) Estimated free hydrogel height vs. time for a 1.5 mm hydrogel cube in SGF and SIF (n = 3, error bars are standard deviation). Note: Capsule images in fluid were rotated 90° for better visualization of the capsule states.

to larger opening force than Design A (Fig. 2b and Fig. 2c, magenta line, max. force between step 3 - 5). With smaller opening force on Design A, the capsule remained opened for a few seconds before sampling and closing within 100 ms (i.e., three frames of the 30 frame per second video, Supplementary Video 2) compared to Design B where opening, sampling, and closing occurred within 33.3 ms (i.e., one frame of the 30 frame per second video, Supplementary Video 2).

C. Hydrogel Actuated Capsule: Hydrogel Height vs. Time, Sampling Volume, h_{crit}, Air Gap

The designs were then tested with hydrogel actuation. Hydrogel height over time was recorded by capturing images of the hydrogel actuated capsule in SGF for 24 hours and then in SIF for 24 hours every 15 seconds (Fig. 6a). The SGF and SIF were dyed with several drops of food coloring for easier visualization of captured sample in the capsule. In SGF, the hydrogel swelled minimally and the hydrogel height was small over time so the mechanism was untriggered. In SIF, the hydrogel height swelled significantly. At 6.9 and 15.2 hours, sampling was triggered for Design A and B respectively (Fig. 6a and Fig. 6b). Design A demonstrated long opening times before fast sampling and closing similar to what was observed in manual actuation most likely due to friction/drag experienced by the piston magnet and lower opening forces (Supplementary Video 2 vs. Supplementary Video 3).

The hydrogel swelling rate in the capsule was slow compared to the hydrogel free swelling rate (Fig. 6b initial slopes vs. Fig. 6c initial slopes respectively). Hydrogel free swelling is when the hydrogel is placed directly in SGF and SIF and allowed to swell freely without any constraints. To obtain the hydrogel height under free swelling, hydrogel mass was measured at 0, 1, 2, 4.5, 19, and 24 hours, converted to volume given the measured initial hydrogel density, and calculated from volume assuming isotropic swelling. From the comparison of the slopes, the mass transfer of fluid into the capsule will need to be improved to increase the hydrogel swelling rate. Regardless, both designs sampled successfully to full volume (Fig. 6a). The air gap for Design A in the hydrogel actuated test was estimated to be approximately 0.95 mm which matched with the average air gap measured in the manual tests in Fig. 5d of 1.03 $\pm$ 0.08 mm (n = 3, mean $\pm$ standard deviation). The air gap for Design B was not captured as the opening, sampling, and closing mechanisms were faster than the camera's frame rate of one frame per 15 seconds.

D. Capsule Locomotion by an External Rotating Magnetic Field

This section explores the locomotion modes of the capsule with an external rotating magnetic field. The net magnetization direction of the capsule is along the short axis of the capsule (Fig. 7a). Three locomotion modes are possible (Fig. 7b). Rotation in a tube and rolling in an unconstrained environment are possible because of friction at contact points between the capsule and surface. Tumbling is possible when the net magnetization direction of the capsule is aligned along the y-axis and the capsule is in a confined space (Fig. 7c). An 8-coil electromagnetic system was used to apply an external rotating magnetic field. The external rotating magnetic field generated a torque on the capsule ($\tau_{\mathbf{capsule}}$) to drive locomotion based on the following equation,

$$\tau_{\mathbf{capsule}} = \mathbf{m_{capsule}} \times \mathbf{B_{ext}} \tag{2}$$

where $\mathbf{m_{capsule}}$ is the net magnetization vector of the capsule and the external rotating magnetic field ($\mathbf{B_{ext}}$) is given by the following equation

$$\mathbf{B_{ext}} = B[\cos(2\pi ft)\cos(\theta)\mathbf{i}+\sin(2\pi ft)\mathbf{j}+\cos(2\pi ft)\sin(\theta)\mathbf{k}], \tag{3}$$

where B, f, t, and θ are the field magnitude, frequency of the rotating magnetic field, time, and azimuth angle respectively. To steer the capsule, the plane of the rotating magnetic field would tilt at an angle of θ towards the heading direction.

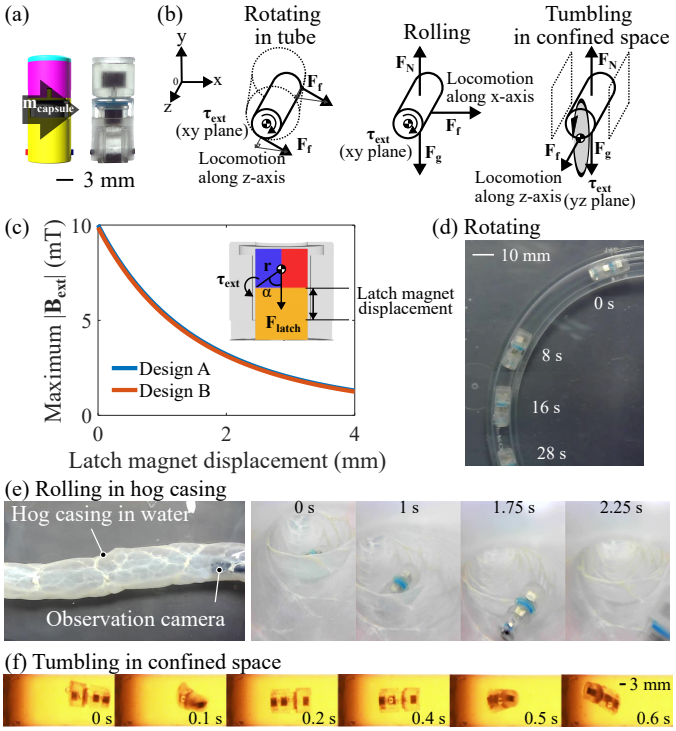

Fig. 7. (a) Capsule render and fabricated capsule showing the net magnetization direction (black arrow along the capsule's short axis). (b) Free body diagrams of capsule rotating in a tube, rolling, and tumbling in a confined space demonstrating friction (F_f) is essential in locomotion. (c) Predicted maximum magnetic field magnitude ($|\mathbf{B_{ext}}|$) for locomotion vs. latch magnet displacement of Design A and B. (d) Design A rotating in a tube using an external rotating magnetic field where the piston magnet is in its untriggered state. (e) Experimental setup of Design A locomotion in an approximately 32 - 35 mm diameter natural hog casing and images of Design A inside the natural hog casing in water rolling towards the camera. (f) Design B tumbling in a tube in SIF.

A misalignment between the external rotating field plane from the capsule's net magnetization direction may cause the latch magnet to rotate out-of-place and prematurely trigger the capsule. The torque balance on the latch magnet will be the sum of the torque by the external magnetic field on the latch magnet and the opposing torque on the latch magnet due to magnetic interaction force among all magnets shown in (4). Inter-magnetic torques on the latch magnet from the other magnets were not considered as the magnetic moments of all magnets are parallel with each other. The torque balance is given as

$$|\mathbf{m}_{\text{latch}}||\mathbf{B}_{\text{ext}}|\sin 90^\circ + |\mathbf{r}||\mathbf{F}_{\text{latch}}|\sin\alpha = 0, \tag{4}$$

where $\mathbf{m}_{\text{latch}}$ is the magnetic moment of the latch magnet, $\mathbf{r}$ is the position vector originating from the bottom left corner of the latch magnet to its COM, $\mathbf{F}_{\text{latch}}$ is the net force on the latch magnet from all other capsule magnets (Fig. 7c). The largest external torque will be when the plane of $\mathbf{B}_{\text{ext}}$ is perpendicular to $\mathbf{m}_{\text{latch}}$. From (4), the external magnetic field magnitudes that would rotate the latch magnet around its bottom left corner for Design A and B were calculated. A field magnitude less than 10 mT would ensure that the latch magnet would not be rotated and prematurely trigger the sampling mechanism (Fig. 7c). Moreover, the capsule structure physically prevents undesired torques for the latch and piston magnets to minimize the premature actuation of the sampling mechanism while magnetic locomotion is used. Impact forces on the capsule are more likely to prematurely trigger capsule sampling especially as the latch magnet reaches h_{crit} where the net clamping force decreases (F_{upper}, Fig. 2b and Fig. 2c, magenta line 1 - 3).

In all locomotion modes, the sampling mechanism remained untriggered with an external field magnitude $<$ 10 mT when the capsule was at its initial configuration. Fig. 7d and Fig. 7e shows Design A rotating in a plastic tube and rolling in natural hog casings under water (approximately 32 - 35 mm diameter) to simulate an adult pig's small intestine environment under a field magnitude of 9 mT and frequency of 3 Hz. The rolling capsule moved faster than the capsule constrained in the tube (Supplementary Video 4). Tumbling motion was conducted in a plastic tube with a diameter of 26.3 mm at field magnitudes of 3 mT and frequency of 1 Hz (Fig. 7f).

E. Capsule Locomotion and Sampling

Assuming smooth and no slip rolling, the capsule's translation speed is as follows

$$v = \omega_c r_c, \omega_c < \omega_{step}, \tag{5}$$

where v, ω_c, r_c, and ω_{step} are the capsule's translation/rolling speed, rotational speed, radius, and step-out rotational speed which is usually experimentally determined. Assuming synchronicity between the external rotating field and the capsule's magnetic moment, the rotational speed of the capsule can be derived from the frequency (f) of the external rotating field as

$$\omega_c = 2\pi f. \tag{6}$$

The capsule's rolling speed as a function of frequency and magnetic field magnitude were characterized by having the capsule roll back and forth in water (Fig. 8a). From the video, the capsule's position was tracked using MATLAB's image processing functions and the capsule speed was calculated by taking the slope of the capsule's distance versus time. Using (5) and (6), the rolling speed of the capsule can be predicted before the step-out frequency is reached and aligns with the data. Fig. 8a demonstrates that above a frequency of 3 Hz, the capsule starts to slip and no considerable gain in rolling speed was achieved. At larger field magnitude of 5 mT, lower speeds were observed compared to 3 mT. As larger frequencies or field magnitudes were used, a wobble around the vertical axis of the capsule was magnified possibly due to uneven torques at the two ends of the capsule and would need further investigation in the future. Therefore, an external rotating magnetic field with frequency 1 Hz and magnitude of 3 mT was used in the subsequent locomotion and sampling test.

First, all air bubbles in the hydrogel compartment of Design B were removed at the start of capsule immersion in SIF to improve fluid mass transfer into the capsule (Fig. 8b, step 1). After 1 hour, the capsule was moved to the target location via

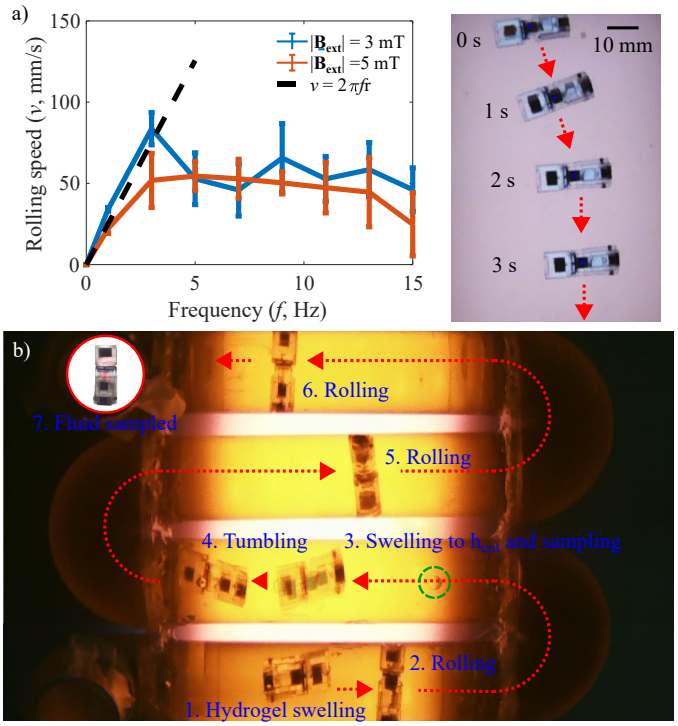

Fig. 8. (a) Capsule rolling speed vs. rotating magnetic field frequency at 3 mT (n = 5) and 5 mT (n = 4) magnetic field magnitude in water and image of Design B rolling in water. (b) Design B locomotion (3 mT, 1 Hz) and sampling in SIF: 1 - Hydrogel is swelling for 1 hour, 2 - The capsule is moved to the target site, 3 - The hydrogel swells to critical hydrogel height at 6.08 hours and samples fluid, 4 - The capsule is moved away from the target site via tumbling, 5 and 6 - The capsule moves towards the exit, 7 - The retrieved capsule successfully sampled fluid without external activation. The green circle shows the air bubble that exited the capsule after sampling.

rolling (Fig. 8b, step 2). At the target location, the hydrogel was allowed to swell to its h_{crit} and the camera's frame rate was set to one frame per 5 seconds (Fig. 8b, step 3). The critical hydrogel was reached 5.08 hours later (Fig. 8b, step 3). The total time-to-trigger of 6.08 hours was lower than the 6.9 and 15.2 hours reported in static sampling tests due to removed air bubbles in the hydrogel compartment prior to swelling. Finally, the camera's frame rate was set to 30 frames per second for real-time video capture and the capsule exited the tube via tumbling and rolling motion. A video of the locomotion and sampling process can be found in Supplementary Video 5 and demonstrates the importance of friction between the capsule and surface contact points for locomotion.

F. Piston and Capsule Seal

In this work, a magnetic micropiston was used to sample fluid via suction. To generate suction force in micropistons, liquid seals have been used due to its low friction compared to traditional contact seals at small scales [34, 35]. A liquid piston seal was used in the sampling compartment to facilitate piston magnet suction for sampling and to function as a capsule seal to prevent sample contamination. Fig. 9 demonstrates the difference between a water seal and vegetable oil seal under static conditions in water. The water seal was dyed with red food coloring to easily visualize the effectiveness of the seal. With the water seal, the external aqueous fluid quickly diluted the water seal after 2 hours. Eventually, the sampling compartment was mostly filled with fluid as evident with the disappearance of the air bubble and color dilution in Fig. 9a. With the oil seal, water did not appear to fill the sampling compartment as evident with the air bubble remaining in the compartment even after 12 hours in Fig. 9b. The aqueous external fluid was dyed with red food colouring in Fig. 9b as the food colouring would be more soluble in aqueous solution rather than in the oil seal. Therefore, all fabricated capsules used a vegetable oil seal to enable piston suction and to provide a better capsule seal compared to water.

G. External Forces on the Capsule

External forces on the capsule could potentially prevent the capsule from opening and/or break its o-ring seal. This section aims to address these concerns. The maximum opening force generated for Design A and B are shown in the Fig. 2b and Fig. 2c by the magenta line for the net force of the upper half of the capsule (F_{upper}) from steps 3 - 5. As the capsule slides open from steps 3 - 5 in Fig. 2d, the F_{upper} increases to a maximum. The maximum opening force exerted by the upper half of the capsule were 46.1 mN and 123.2 mN for Design A and B respectively (Fig. 2b and Fig. 2c). The pressures from the maximum forces for an approximately 6.5 mm diameter sampling compartment would be 1.4 kPa and 3.7 kPa for Design A and B respectively. These pressures would be able to overcome the normal intra-abdominal pressure of an adult of 0.67 - 0.93 kPa [3] for capsule opening.

When comparing the maximum capsule opening force to measured axial and radial forces in the intestines from literature (92 - 300 mN and 0 - 155 mN for a 12 mm diameter capsule respectively [36]), the capsule design parameters will need to be readjusted. Since the current capsule diameter and length are smaller than the maximum recommended size of 11 and 26 mm respectively, it would be possible to scale the capsule to a larger size to achieve larger opening forces to counteract axial forces in the intestines. For example, if all Design B capsule and magnet dimensions were scaled larger from 1 to 1.24 and r_{spring} was decreased with respect to half the activating magnet width ($w_{activate0.5}$), functional designs with opening force greater than 300 mN axial force would be possible (Fig. 10). Note: Scaling factor stops at 1.24 to stay within the recommended capsule length of 26 mm. Alternatively, it would be possible to increase the length of the sliding component by 2 - 3 mm and close the bottom of the sliding component. In doing so, the lower half of the capsule would not be exposed to external forces as it slides open. Thus, any external forces will be only on the capsule's static exterior.

Finally, the o-ring seal pressure limit was compared to the reported intra-abdominal pressures of a healthy adult (IAP). Fig. 11a shows a 3D printed tube (ClearV4, FormLabs Inc.) with a 3.5 × 3.5 mm square channel to simulate the capsule's sampling compartment. A 3 mm cube magnet was placed into the channel and the channel was closed off on one end with a sampling compartment lid. The o-ring seal cured onto a

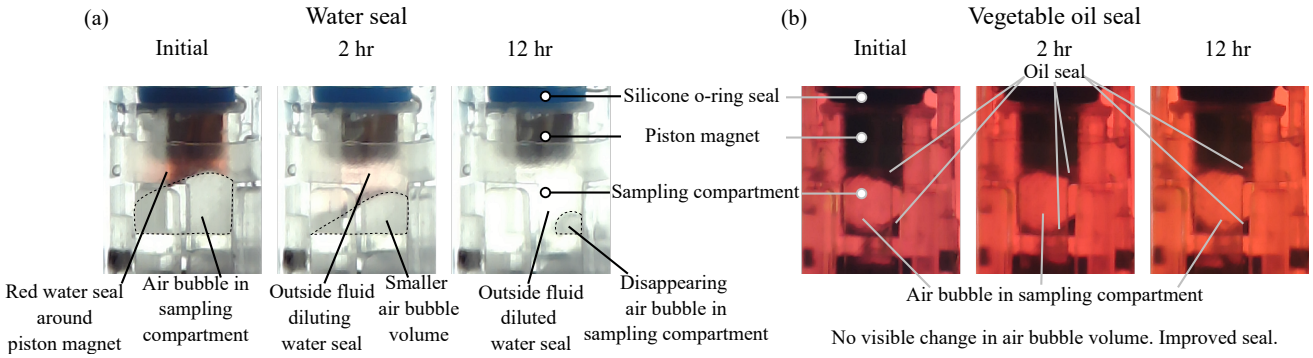

Fig. 9. Zoomed in view of the sampling compartment. Comparison of (a) water seal with red food coloring around the piston magnet in the sampling compartment and (b) vegetable oil seal around piston magnet in the sampling compartment. The sampling compartment was immersed in deionized water for the water seal test and deionized water with red food coloring for the vegetable oil seal test.

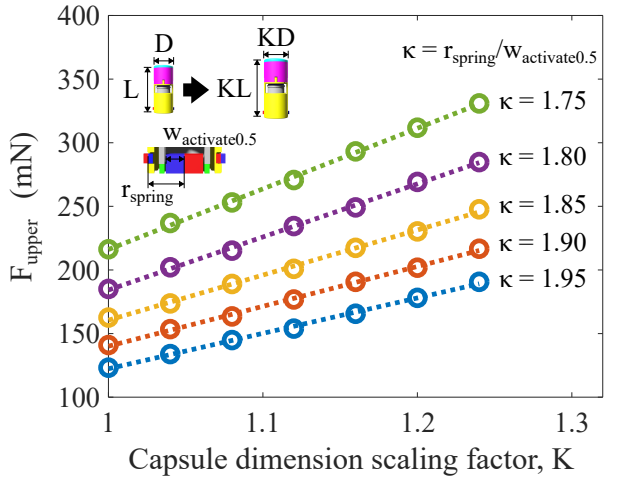

Fig. 10. Predicted maximum opening force of the capsule (F_{upper} in mN when the capsule is opening) vs. capsule dimensions scaling factor (K) for Design B where κ is the ratio of r_{spring} over $w_{activate0.5}$. A larger κ means the spring magnet is positioned further away from the axis of the cylindrical capsule.

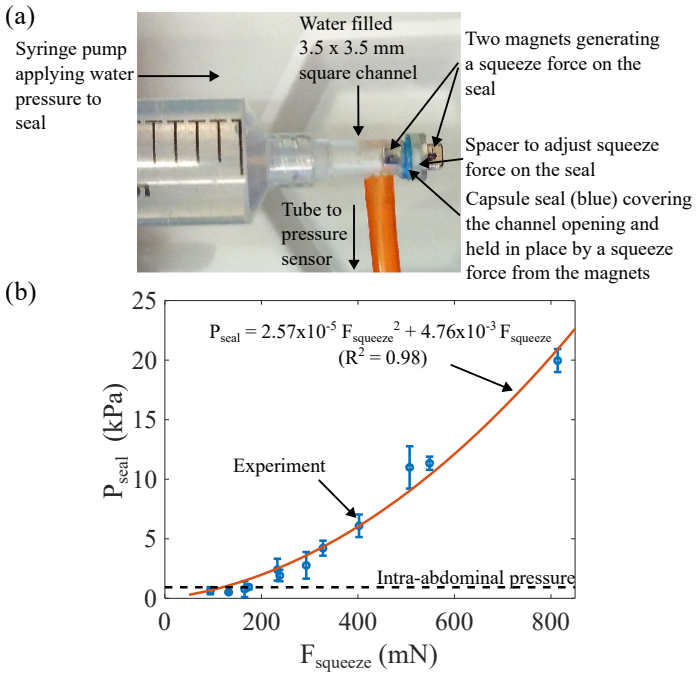

Fig. 11. (a) Experimental set-up to measure o-ring seal pressure limit of the capsule. (b) Seal pressure limit (P_{seal} in kPa) vs. seal squeeze force ($F_{squeeze}$ in mN) with fitted curve (red) and experimental data (n = 3, error bars are standard deviation). Black dotted line represents the upper limit of the intra-abdominal pressure in a healthy adult (0.93 kPa).

3D printed spacer with Mold Star 30 (0.5 mm thick) was placed over the sampling compartment lid. Another magnet of varying sizes and with opposite magnetization direction from the channel magnet was placed on the spacer to apply a squeeze force on the seal. Magnetic dipole model was used to calculate the varying squeeze force between the two cube magnets on the o-ring seal. Additional 3D printed spacers with set thicknesses of 1, 1.5, 2, and 2.5 mm were placed between the magnets to adjust the squeeze force. The other end of the square channel tube was attached to a syringe filled with water. A syringe pump (NE-1000, New Era Pump Systems) pumped the water at a rate of 1 mL·min^{-1} into the channel. A pressure sensor (SparkFun Qwiic MicroPressure Sensor, Sparkfun Electronics) was placed just before the seal area to measure the maximum seal gauge pressure before the pressure dropped.

The capsule's squeeze force on the seal depends on the capsule's closing force. The initial and final closing force of the capsule are different. The final capsule closing force after sampling would be larger than the initial closed capsule force, enabling better squeeze force on the o-ring seal to minimize sample contamination after fluid sampling. The capsule closing force can be calculated from the net force of the entire upper half of the capsule according to

$$F_{\text{upper}} = \begin{cases} F_{\text{latch}} + F_{\text{spring}}, & \text{(initially closed capsule)} \\ F_{\text{latch}} + F_{\text{spring}} + F_{\text{piston}}, & \text{(final closed capsule).} \end{cases} \quad (7)$$

For Design A and B, the initial closing forces were -198 mN and -180 mN respectively compared to -408 mN and -742 mN for the final closed capsule forces respectively (Fig. 2b and Fig. 2c, capsule step 1 vs. 7). From Fig. 11b, these force magnitudes translate to the o-ring seal pressure limit of 1.95, 1.69, 6.23, and 17.7 kPa respectively which are greater than the reported upper IAP limit of a healthy adult of 0.93 kPa [3].

V. Discussion and Future Work

Two designs were shown to automatically sample SIF and were externally controlled for active locomotion. The piston oil seal was effective in preventing leakage and sample contamination. The silicone rubber o-ring seal was able to withstand normal intra-luminal abdominal pressures. However, the sliding mechanism was prone to friction and capillary forces, leading to smaller capsule openings (i.e., smaller air gaps) than predicted. Second, the capsule opening force of Design B could only overcome the lower range of reported external axial and radial intestinal force. However, it was shown that design parameters like magnet dimensions and r_{spring} can be adjusted for larger opening forces. Moreover, the sliding compartment design can also be adjusted to protect the sliding lower half of the capsule from being exposed to external forces when opening. Third, the sampling compartment volume was relatively small in comparison to other hydrogel capsule designs (31 µL and 41 µL for an overall capsule size of 8 mm $\times$ 19 mm and 8 mm $\times$ 21 mm vs. sampling volume of 200 µL - 300 µL for an overall capsule size of 7 mm × 11 mm [23] and 9 mm $\times$ 26 mm [21]). The sampling volumes were also smaller than the magnetically actuated capsules in [16, 17] (42 µL for a 8 mm × 11 mm capsule and 1500 µL for a 12.4 mm $\times$ 26 mm capsule respectively). However, by sacrificing sampling volume, an independent sampling compartment from the hydrogel was possible, enabling easy sample extraction from the capsule.

Other limitations in this work would be that significant microbiome populations reside not in the intestinal fluid but in the mucosal layer surrounding the edge of the intestine. Methods to collect from the mucosa could be beneficial. For example, future capsule designs can be coated with a soft brush or helix which can rotate against the intestines to release particulates from the intestinal mucosa for sampling similar to [37]. However, it is unknown whether the piston suction force would be sufficient in sampling more viscous or solid particulates which should be further studied.

Piston suction force for sampling is related to piston seal performance. In this work, all seal and sampling tests were performed statically. It will be valuable to study the capsule's seal performance under a dynamic environment and to observe whether the capsule will prematurely trigger from the peristaltic motion of the gut. Such earlier triggering in the intestines is not however necessarily undesirable as the fluid sampling mechanism in the experiments was triggered after 6 - 15 hours in SIF. The trigger time for this capsule may be too long for the average 4 - 6 hour transit time in the small intestine [3, 23]. Although the time-to-trigger the sampling mechanism was slow, the sampling and closing mechanism occurred in $<$ 5 seconds in the final locomotion and hydrogel actuated sampling tests. This sampling time is much faster than other hydrogel actuated capsules which took 3 - 4 minutes [21, 29] and an hour [22] prior to capsule closing because it took time for the hydrogel to collect sample and seal the capsule. Thus, the hydrogel swelling rate in this work only affected the time-to-trigger and not sampling and closing times in comparison to other hydrogel actuated capsules [21, 22, 29].

Lowering the time-to-trigger within the average intestinal transit time can be further investigated by: (i) lowering the h_{crit} constraint in design space exploration to reach h_{crit} faster without modifying the hydrogel material, (ii) coating the channels in the hydrogel compartment with poly(ethylene glycol) for faster surface wetting to enable faster fluid mass transfer to the hydrogel, or (iii) lowering hydrogel crosslinking by lowering curing time and re-characterizing the material's blocking force and mechanical properties. Moreover, add-on features like magnetic localization, anchoring, and locomotion can be further explored to help with site-specific sampling and possible capsule retention issues.

Finally, the hydrogel actuator is pH-dependent and a question that may arise is the body's ability to maintain gut homeostasis in terms of gastric and intraluminal pH. The hydrogel only exhibits large volume transition at pH $>$ 6 as investigated in [31] and the capsule is designed to trigger at h_{crit} between the maximum hydrogel height in SGF (pH 1.2) and SIF (pH 6.8) at low salt concentrations. Assuming that SGF and SIF are good representations of the average gastric and intestinal pH and salt conditions and given a healthy body's natural propensity for maintaining gut homeostasis in the stomach (pH 1.2 - 3) and in the intestines (pH 6.6 - 7.5 depending on the duodenum, ileum, or jejunum) [3], the capsule will trigger in the intestines. Otherwise, large deviation from homeostasis may signify critical illness that may need to be more immediately addressed than proceeding with sampling operations. For example, gut sepsis may lead to intraluminal pH shifts and will increase certain bacterial populations and their virulence leading to increased patient mortality [38]. Chronic pancreatitis may cause low intraluminal pH due to bile acid malabsorption in the intestines [39]. *H. pylori* infection in the stomach can lead to inflammation causing peptic ulcers, gastritis, hypochlorhydria (lower gastric acid secretion which can increase gastric pH), and gastric adenocarcinoma [40]. Meanwhile, the effect of IBD on intraluminal pH was inconclusive with some studies showing patients with pH deviations and some without [41]. The application of the capsules in patients with varying chronic gut diseases will need to be studied to determine whether pH deviations exist and will also be a useful marker of gut disease [38] but out of the scope of this paper.

VI. Conclusion

The study presents the design of a hybrid hydrogel-magnet actuated fluid sampling capsule. It features automatic targeted sampling in the intestines without enteric coating and active locomotion while maintaining a relatively small size of 8 mm $\times$ 19 mm and 8 mm $\times$ 21 mm with an independent sampling compartment from the hydrogel. Moreover, preliminary seal characterization demonstrates sample contamination mitigation. While the time-to-trigger the mechanism is slow (6 - 15 hours), optimization of the pH-responsive hydrogel swelling rate or hydrogel compartment design will enable trigger times within the average intestinal transit time. Finally, further work exploring its locomotion and anchoring features will enable improved targeted sampling in the intestines.

REFERENCES

[1] W. M. de Vos, *et al.*, "Gut microbiome and health: mechanistic insights," *Gut*, vol. 71, no. 5, pp. 1020–1032, 2022.

[2] J. S. Biteen, *et al.*, "Tools for the microbiome: Nano and beyond," *ACS Nano*, vol. 10, no. 1, pp. 6–37, 2016.

[3] L. Barducci, *et al.*, "Fundamentals of the gut for capsule engineers," *Prog. Biomed. Eng.*, vol. 2, no. 4, p. 042002, 2020.

[4] G. Iddan, *et al.*, "Wireless capsule endoscopy," *Nature*, vol. 405, no. 6785, pp. 417–417, 2000.

[5] M. Simi, *et al.*, "Magnetic torsion spring mechanism for a wireless biopsy capsule," *J. Med. Devices*, vol. 7, no. 4, p. 041009, 2013.

[6] S. Yim, *et al.*, "Biopsy using a magnetic capsule endoscope carrying, releasing, and retrieving untethered microgrippers," *IEEE Trans. Biomed. Eng.*, vol. 61, no. 2, pp. 513–521, 2014.

[7] M. C. Hoang, *et al.*, "Untethered robotic motion and rotating blade mechanism for actively locomotive biopsy capsule endoscope," *IEEE Access*, vol. 7, pp. 93 364–93 374, 2019.

[8] D. Son, H. Gilbert, and M. Sitti, "Magnetically actuated soft capsule endoscope for fine-needle biopsy," *Soft Robot.*, vol. 7, no. 1, pp. 10–21, 2020.

[9] J. Cui, *et al.*, "The study of a remote-controlled gastrointestinal drug delivery and sampling system," *Telemed. e-Health*, vol. 14, no. 7, pp. 715–719, 2008.

[10] S. Yim and M. Sitti, "Design and rolling locomotion of a magnetically actuated soft capsule endoscope," *IEEE Trans. Robot.*, vol. 28, no. 1, pp. 183–194, 2012.

[11] V. H. Le, *et al.*, "A soft-magnet-based drug-delivery module for active locomotive intestinal capsule endoscopy using an electromagnetic actuation system," *Sens. Actuators A Phys.*, vol. 243, pp. 81–89, 2016.

[12] A. Chiba, *et al.*, "Magnetic actuator for a capsule endoscope navigation system," *J. Magn.*, vol. 12, no. 2, pp. 89–92, 2007.

[13] P. Valdastri, *et al.*, "A new mechanism for mesoscale legged locomotion in compliant tubular environments," *IEEE Trans. Robot.*, vol. 25, no. 5, pp. 1047–1057, 2009.

[14] D. Becker, *et al.*, "Novel orally swallowable Intellicap® device to quantify regional drug absorption in human GI tract using Diltiazem as model drug," *AAPS PharmSciTech*, vol. 15, no. 6, pp. 1490–1497, 2014.

[15] M. Rehan, *et al.*, "Development of a robotic capsule for in vivo sampling of gut microbiota," *IEEE Robot. Autom. Lett.*, vol. 7, no. 4, pp. 9517–9524, 2022.

[16] P. Shokrollahi, *et al.*, "Blindly controlled magnetically actuated capsule for noninvasive sampling of the gastrointestinal microbiome," *IEEE/ASME Trans. Mechatron.*, vol. 26, no. 5, pp. 2616–2628, 2021.

[17] J. Nam, *et al.*, "Resonance-based design of wireless magnetic capsule for effective sampling of microbiome in gastrointestinal tract," *Sens. Actuators A Phys.*, vol. 342, p. 113654, 2022.

[18] S. Park, *et al.*, "Active multiple-sampling capsule for gut microbiome," *IEEE/ASME Trans. Mechatron.*, vol. 27, no. 6, pp. 4384–4395, 2022.

[19] H. An, *et al.*, "pH sensor-embedded magnetically driven capsule for H. pylori infection diagnosis," *IEEE Robot. Autom. Lett.*, vol. 7, no. 4, pp. 9067–9074, 2022.

[20] M. Finocchiaro, *et al.*, "Design of a magnetic actuation system for a microbiota-collection ingestible capsule," in *2021 IEEE International Conference on Robotics and Automation (ICRA)*, 2021, pp. 6905–6911.

[21] M. Ben Salem, *et al.*, "Microbiota sampling capsule: Design, prototyping and assessment of a sealing solution based on a bistable mechanism," *J. Med. Devices*, vol. 16, no. 4, p. 041009, 2022.

[22] J. F. Waimin, *et al.*, "Smart capsule for non-invasive sampling and studying of the gastrointestinal microbiome," *RSC Adv.*, vol. 10, pp. 16 313–16 322, 2020.

[23] S. Nejati, *et al.*, "Smart capsule for targeted proximal colon microbiome sampling," *Acta Biomater.*, vol. 154, pp. 83–96, 2022.

[24] S. Babaee, *et al.*, "Temperature-responsive biometamaterials for gastrointestinal applications," *Sci. Transl. Med.*, vol. 11, no. 488, p. eaau8581, 2019.

[25] L. Hines, *et al.*, "Soft actuators for small-scale robotics," *Adv. Mater.*, vol. 29, no. 13, p. 1603483, 2017.

[26] X. Liu, *et al.*, "Ingestible hydrogel device," *Nat. Commun.*, vol. 10, no. 1, p. 493, 2019.

[27] H. Banerjee and H. Ren, "Optimizing double-network hydrogel for biomedical soft robots," *Soft Robot.*, vol. 4, no. 3, pp. 191–201, 2017.

[28] H. Jiang, *et al.*, "A smart capsule with a hydrogel-based pH-triggered release switch for GI-tract site-specific drug delivery," *IEEE Trans. Biomed. Eng.*, vol. 65, no. 12, pp. 2808–2813, 2018.

[29] M. Ben Salem, *et al.*, "Design of a microbiota sampling capsule using 3D-printed bistable mechanism," in *2018 40th Annual International Conference of the IEEE Engineering in Medicine and Biology Society (EMBC)*, 2018, pp. 4868–4871.

[30] A. Fritscher-Ravens, *et al.*, "The feasibility of wireless capsule endoscopy in detecting small intestinal pathology in children under the age of 8 years: a multicentre European study," *Gut*, vol. 58, no. 11, pp. 1467–1472, 2009.

[31] Y. P. Lai, *et al.*, "Hybrid hydrogel-magnet actuators with pH-responsive hydrogels for gastrointestinal microrobots," *Adv. Eng. Mater.*, p. 2301060, 2023.

[32] A. J. Petruska and J. J. Abbott, "Optimal permanent-magnet geometries for dipole field approximation," *IEEE Trans. Magn.*, vol. 49, no. 2, pp. 811–819, 2013.

[33] M. W. Ariefdjohan, D. A. Savaiano, and C. H. Nakatsu, "Comparison of DNA extraction kits for PCR-DGGE analysis of human intestinal microbial communities from fecal specimens," *Nutr. J.*, vol. 9, no. 1, p. 23, 2010.

[34] M. De Volder, *et al.*, "A novel hydraulic microactuator sealed by surface tension," *Sens. Actuators A Phys.*, vol. 123-124, pp. 547–554, 2005.

[35] A. Barbot, *et al.*, "Liquid seal for compact micropiston actuation at the capillary tip," *Sci. Adv.*, vol. 6, no. 22, p. eaba5660, 2020.

[36] M. Rehan, *et al.*, "Measurement of peristaltic forces exerted by living intestine on robotic capsule," *IEEE/ASME Trans. Mechatron.*, vol. 26, no. 4, pp. 1803–1811, 2021.

[37] S. S. Srinivasan, *et al.*, "Robocap: Robotic mucus-clearing capsule for enhanced drug delivery in the gastrointestinal tract," *Sci. Robot.*, vol. 7, no. 70, p. eabp9066, 2022.

[38] I. Fleming, *et al.*, *Critical illness and the intestinal Microflora: pH as a surrogate marker*. New York, NY: Springer New York, 2014, pp. 1–9.

[39] R. Pezzilli, "Chronic pancreatitis: maldigestion, intestinal ecology and intestinal inflammation," *World J. Gastroenterol.*, vol. 15, no. 14, pp. 1673–1676, 2009.

[40] A. J. Smolka and S. Backert, "How helicobacter pylori infection controls gastric acid secretion," *J. Gastroenterol.*, vol. 47, no. 6, pp. 609–618, 2012.

[41] S. G. Nugent, *et al.*, "Intestinal luminal pH in inflammatory bowel disease: possible determinants and implications for therapy with aminosalicylates and other drugs," *Gut*, vol. 48, no. 4, pp. 571–577, 2001.